The Royal Society of Victoria, 130, 32–49, 2018
10.1071/RS18005

THE MOYJIL SITE, SOUTH-WEST VICTORIA, AUSTRALIA: CHRONOLOGY

John E. Sherwood[1], Jim M. Bowler[2], Stephen P. Carey[3], John Hellstrom[2], Ian J. McNiven[4], Colin V. Murray-Wallace[5], John R. Prescott[6], Daniele G. Questiaux[7], Nigel A. Spooner[7], Frances M. Williams[8] and Jon D. Woodhead[2]

[1]School of Life and Environmental Sciences, Deakin University, Warrnambool, Victoria 3280, Australia
[2]School of Earth Sciences, University of Melbourne, Victoria 3010, Australia
[3]School of Science, Engineering and Information Technology, Federation University Australia, Ballarat, Victoria 3353, Australia
[4]ARC Centre of Excellence for Australian Biodiversity and Heritage, Monash Indigenous Studies Centre, Monash University, Melbourne, Victoria 3800, Australia
[5]School of Earth and Environmental Sciences, University of Wollongong, NSW 2522, Australia
[6]deceased, formerly University of Adelaide, Adelaide, South Australia 5005, Australia
[7]Prescott Environmental Luminescence Laboratory (PELL), School of Physical Sciences, and Institute for Photonics and Advanced Sensing (IPAS), University of Adelaide, Adelaide, South Australia 5005, Australia
[8]Prescott Environmental Luminescence Laboratory (PELL), School of Physical Sciences, and Institute for Photonics and Advanced Sensing (IPAS), and Department of Earth Sciences, University of Adelaide, Adelaide, South Australia 5005, Australia

Correspondence: John Sherwood, john.sherwood@deakin.edu.au

ABSTRACT: An unusual shell deposit at Moyjil (Point Ritchie), Warrnambool, in western Victoria, has previously been dated at 67±10 ka and has features suggesting a human origin. If human, the site would be one of Australia's oldest, justifying a redetermination of age using amino acid racemisation (AAR) dating of *Lunella undulata (*syn*. Turbo undulatus)* opercula (the dominant shellfish present) and optically stimulated luminescence (OSL) of the host calcarenite. AAR dating of the shell bed and four Last Interglacial (LIG) beach deposits at Moyjil and Goose Lagoon, 30 km to the west, confirmed a LIG age. OSL analysis of the host sand revealed a complex mixing history, with a significant fraction (47%) of grains giving an early LIG age (120–125 ka) using a three-component mixing model. Shell deposition following the LIG sea-level maximum at 120–125 ka is consistent with stratigraphic evidence. A sand layer immediately below the shell deposit gave an age of ~240 ka (i.e. MIS 7) and appears to have been a source of older sand incorporated into the shell deposit. Younger ages (~60—80 ka) are due to bioturbation before calcrete finally sealed the deposit. Uranium/thorium methods were not applicable to *L. undulata* opercula or an otolith of the fish *Argyrosomus hololepidotus* because they failed to act as closed systems. A U-Th age of 103 ka for a calcrete sheet within the 240 ka sand indicates a later period of carbonate deposition. Calcium carbonate dripstone from a LIG wave-cut notch gave a U–Th age of 11–14 ka suggesting sediment cover created a cave-like environment at the notch at this time. The three dating techniques have collectively built a chronology spanning the periods before and after deposition of the shell bed, which occurred just after the LIG sea-level maximum (120–125 ka).

Keywords: *Turbo undulatus*, *Lunella undulata*, amino acid racemisation, optically stimulated luminescence, laser ablation, uranium/thorium analysis, Point Ritchie

Point Ritchie (called 'Moyjil' by local Aboriginal people) is a rocky headland on the western bank of the Hopkins River mouth (Figure 1) at Warrnambool in western Victoria, Australia (latitude: 38°24'7"S; longitude142°30'29"E). The headland stratigraphy has been described elsewhere (Nair & Sherwood 2007; Carey et al. 2018). Of particular interest here is a sand deposit identified as unit Q2 in Carey et al. (2018) and as the Headland Bed in Nair and Sherwood (2007). Unit Q2 contains charcoal and discoloured (blackened) stones in association with marine molluscan, crustacean and fish remains in terrestrial sands, suggesting that this could be a site of human occupation. When the late E.D. Gill first investigated the site in 1981, the degree of cementation of unit Q2 and its location beneath a calcrete and the Tower Hill Tuff suggested a pre-Holocene age. Subsequent conventional C-14 dating of a range of materials — charcoal, calcrete, and aragonitic and calcitic shell — indicated an age beyond the limit of the radiocarbon method (Gillespie 2002).

Other techniques applicable to materials older than ~40 ka have been used on shell and sediment from Moyjil and other reference sites within the region (Sherwood et al. 1994; Prescott & Sherwood 1988; Goede 1989; Oyston 1996). Amino acid racemisation (AAR) dating and electron spin resonance dating (ESR) give relative age estimates with samples grouped into 'zones' of increasing

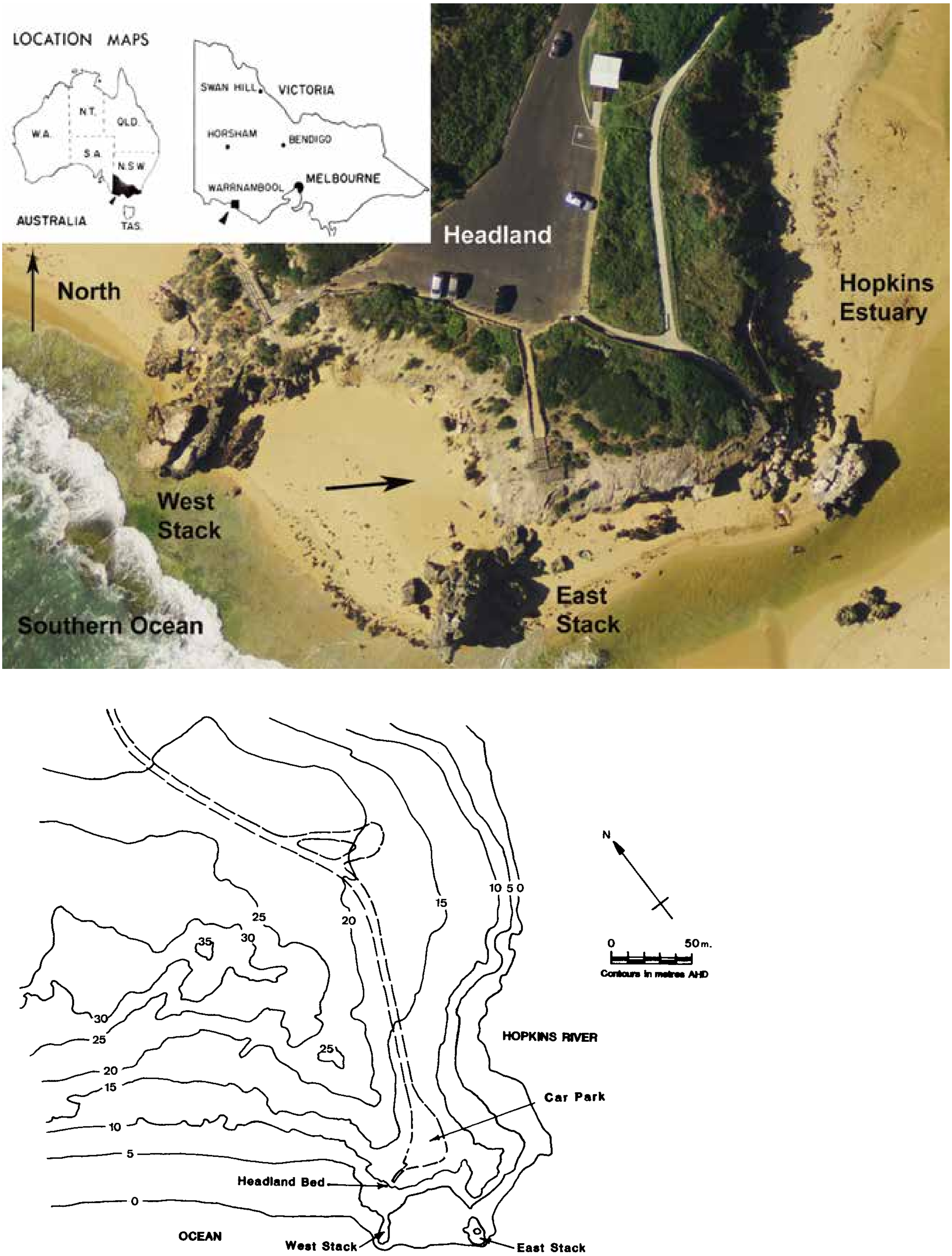

Figure 1: (Top) Aerial photograph of Moyjil (Point Ritchie) south-west Victoria, Australia. The central arrow indicates the direction from which Figure 2 was taken. East and West Stacks are separated by 50 m. Photograph courtesy Aboriginal Victoria. (Bottom) Contour map of the headland area showing the large coastal palaeodune (the Dennington dune) to the north. Contours in metres AHD.

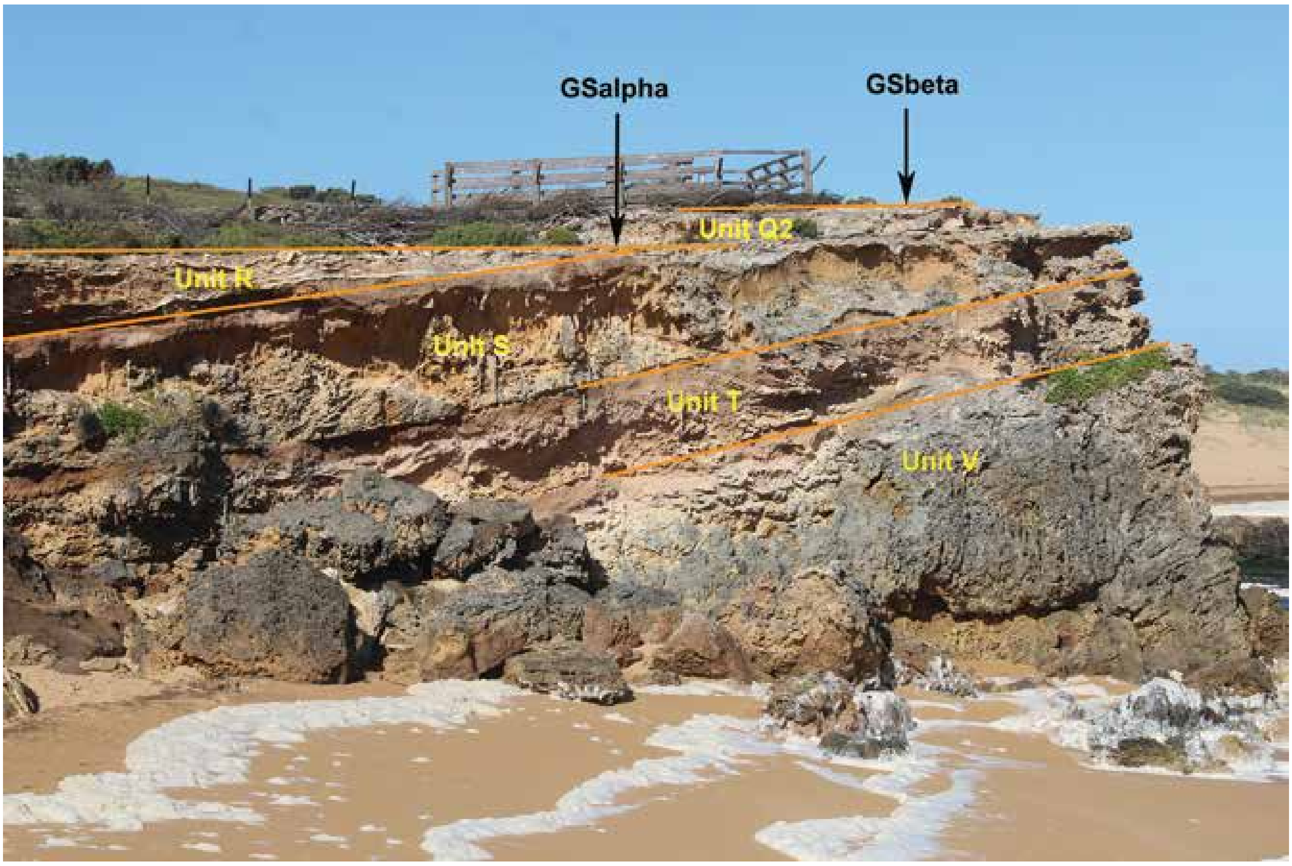

Figure 2: Major stratigraphic units of the Moyjil headland. Photograph of the headland opposite East Stack (see Figure 1). Photograph taken from the beach between the two stacks, looking east. GS = Ground Surface (see text for details). Photograph: J. Sherwood

age. Thermoluminescence (TL) and uranium series (U-series) techniques are capable of giving numerical ages when specific criteria are met. In summary, AAR indicated an age for Moyjil between the Holocene and the Last Interglacial (LIG; Sherwood et al. 1994); U-series dating was not applicable since the shells at Moyjil did not behave as closed systems (Sherwood et al. 1994); ESR dating suggested a late LIG age (Goede 1989); and TL gave age estimates of 67±10 ka (Sherwood et al. 1994) and 80±10 ka and 93±11 ka (Oyston 1996) broadly consistent with the ESR and AAR analyses.

The potential significance of the site (possibly human) and the development of new techniques provided the rationale for a re-investigation of the age of the shell deposit. We report here the results of three new determinations of the age of this site. Refinements in U-series dating using laser ablation techniques and discovery of a new datable fossil (a fish otolith) justified a re-examination of the technique's applicability to Moyjil. Single-grain optically stimulated luminescence (OSL), developed since the initial dating work, has been applied to quartz grains from the site's calcareous sand host. In addition, we have expanded the number of sites studied using amino acid racemisation to better define the relative ages of the Moyjil site and other storm beach deposits.

STRATIGRAPHIC SUMMARY

The deposits at Moyjil/Point Ritchie belong predominantly to two Pleistocene formations: the Bridgewater Formation derived from coastal aeolian dunes and Tower Hill Tuff sourced to a volcanic eruption at 35 ka (Sherwood et al. 2004). These are overlain by Holocene aeolian sands (Figures 2 and 3). We have employed an informal alphabetic subdivision of the Bridgewater Formation and associated units at Moyjil. The relevant stratigraphy is summarised below and described in greater detail elsewhere (Carey et al. 2018). In addition, two important erosional surfaces are identified within the succession and are referred to as Ground surfaces α and β (Gsα, Gsβ).

From bottom to top in the cliff section the relevant informal units are:

- **Unit V** consists of calcarenite with a palaeosol at the top. Its exposed thickness reaches a maximum of 10 m, and shows pronounced variation reflecting the form of a coastal sand dune.
- **Unit T** is a cross-bedded calcarenite with upper palaeosol containing blackened centimetre-scale clasts and common root casts, and is up to 3.5 m thick.
- **Unit S** is a sub-horizontally bedded calcarenite with common root casts, minor conglomerate and an upper palaeosol, with a maximum thickness approaching 3 m.

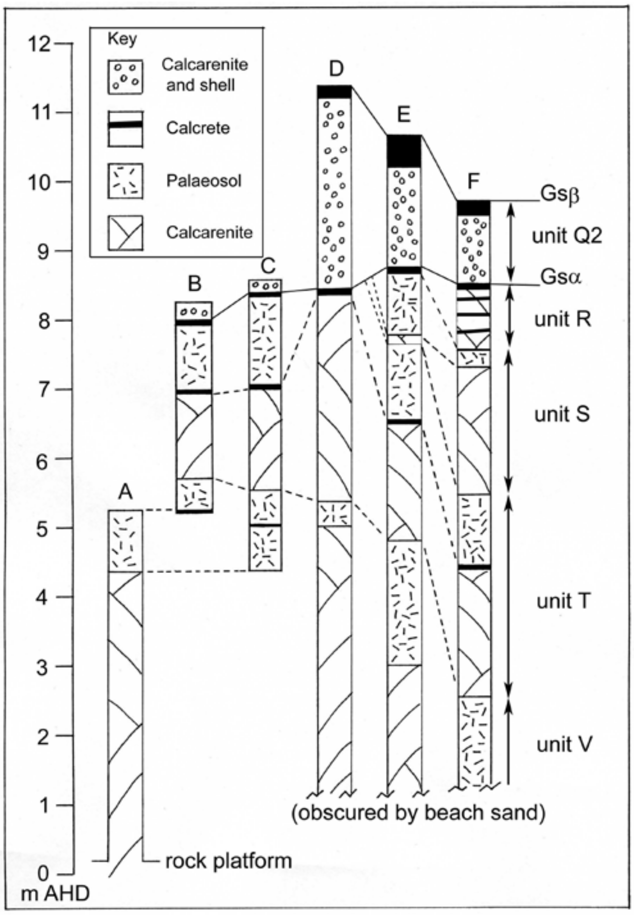

Figure 3: Schematic vertical sections of West Stack and the headland. A – remnant West Stack ridge; B – reconstructed West Stack South (WsS); C – reconstructed West Stack North (WsN); D – headland adjacent to West Stack ridge; E– headland ca. 15 m east of D and near where MR1 – MR3 samples were taken from unit Q2; F – headland ca. 35 m east of D and close to where sample MR4 was taken from unit R.

- **Unit R** is also a calcarenite but, in addition, has multiple calcrete layers, one at its top (Rcs) and others as thin sheets within the unit or at its base (identified as Rcp). Rcs is pedogenic and Rcp is heterogeneous, part showing a microbial influence and part phreatic (groundwater-related). Unit R is up to 1.4 m thick, but over much of the headland the only portion of it preserved is the lower calcrete, Rcp.
- **Gsα** is a horizontal erosional surface at the base of unit Q2 which truncates unit R as deeply as Rcp. Many fire-related features (blackened and fractured stones, charcoal) are concentrated on this surface. A dense shell scatter dominated by fragments of the mollusc *Lunella undulata* (syn. *Turbo undulatus*) as well as discoloured stones occurs on this surface on West Stack.
- **Unit Q2** is a calcareous sand capped with a discontinuous calcrete (Q2cs), the remnant of a palaeosol. The unit has a maximum exposed thickness of 2 m and is the uppermost unit of the Bridgewater Formation. Distributed throughout unit Q2 are occasional molluscan and other marine fossils and some fire-related features (charcoal and discoloured stones).
- **Gsβ** is a second horizontal erosional surface which separates units P and Q2, and which is developed across the top of the calcrete, Q2cs.
- **Unit P** is weathered and partly pedified Tower Hill Tuff occurring on the eastern side of the headland and deposited directly upon unit Q2cs. About 200 m upstream in the Hopkins estuary layered tuff rests on a *terra rossa*, presumed to be a remnant of the soil above Q2cs.

All of these units and surfaces are exposed in the headland at Moyjil but only units Q2 (very thin), Rcp, T, and V, and Gsα are present on West Stack. Stratigraphic correlation of the shells on West Stack with those in the headland's unit Q2 is based on:

- The near identical elevation (8.2 ± 0.2 m AHD) of the surface of West Stack and the headland's Gsα when West Stack blocks are restored to their original positions (Figure 3).
- The horizontal surface of a restored West Stack (shown before collapse in a 1907 postcard; Carey et al. 2018) is less than 15 m from the horizontal Gsα of the headland.
- The observation that, at their closest proximity, Gsα on the headland and the surface of West Stack are underlain by a calcrete and units T and V (Figure 3).
- The occurrence of blackened stones upon calcrete Rcp on both West Stack and the headland.
- The predominance of shells of *L. undulata* and *Sabia conica* at each location and their lack of water-rounded surfaces.
- The determination that shells on both West Stack and in unit Q2 have ages beyond the limit of C-14 (one shell from the headland, four from West Stack; Sherwood et al. 1994; Nair & Sherwood 2007) and occupy the same LIG aminozone (four shells from West Stack, two from the headland; AAR ratios subsequently averaged in Sherwood et al. 1994).

A LIG age for shells on West Stack is further supported by the presence there of a *Lunella torquata* (syn. *Turbo torquatus*) operculum, considered a LIG index fossil for western Victoria (Valentine 1965). Goede (1989) measured equivalent doses (D_e) for *L. undulata* shells during electron spin resonance analysis. Two Moyjil LIG beach deposits yielded similar D_e (three samples – 126, 149, 176 Gray) to a single West Stack shell (D_e = 106 Gray). Goede (1989) concluded all shells were from the LIG with West Stack shells possibly younger than the LIG beach deposits.

Nine remnant storm beach deposits at Moyjil (identified by us as unit Q1) are located between 2 m and 6 m AHD including one located on a calcarenite stack midstream at the present estuary mouth. These vary from well-developed notches filled with rounded boulders and cobbles, shell fragments and sand to thin veneers of sand, gravel and shell plastered on underlying calcarenite. They suggest the headland had a substantial LIG beach immediately to its south and east, which almost completely surrounded East and West Stacks.

METHODS

A note on taxonomy

The World Register of Marine Species (WoRMS Editorial Board 2018) does not currently list the marine molluscs cited here by names formerly accepted within Australia. *Turbo undulatus* and *Turbo torquatus* are placed in the genus *Lunella — as L. undulata* and *L. torquata.* We have retained former species names alongside the WoRMS designations in this paper in order to maintain connectivity with extensive Australian literature using the former names.

U-series dating

U–Th geochronology was attempted on five samples in the School of Earth Sciences at the University of Melbourne (Figure 4). Three samples were from unit Q2:

- A *L. undulata* operculum (operculum 1) from the unit Q2 sand deposit on the headland (diameter 1.8 cm).
- A *L. undulata* operculum (operculum 2) from the shell–sand matrix on the surface (Gsα) of West Stack (diameter 1.9 cm).
- An otolith, identified as coming from the fish *Argyrosomus hololepidotus* (Mulloway) recovered from the headland's unit Q2. From the length of the otolith (2.1 cm) and a plot of otolith length against modern Mulloway mass, the otolith is estimated to come from a fish of 4–6 kg (Nair & Sherwood 2007).

A fourth sample consisted of crystalline calcite recovered from a dripstone formation in a wave-cut notch on the west side of West Stack. The presence of the dripstone indicates the notch was formerly part of a cavern into which groundwater seeped. Fracturing of West Stack into two blocks occurred through the cavern resulting in dripstone being exposed on adjacent faces of the present south and north blocks.

The fifth sample was a crystalline calcrete from the headland's unit Rcp.

Laser ablation trace-element data were first obtained

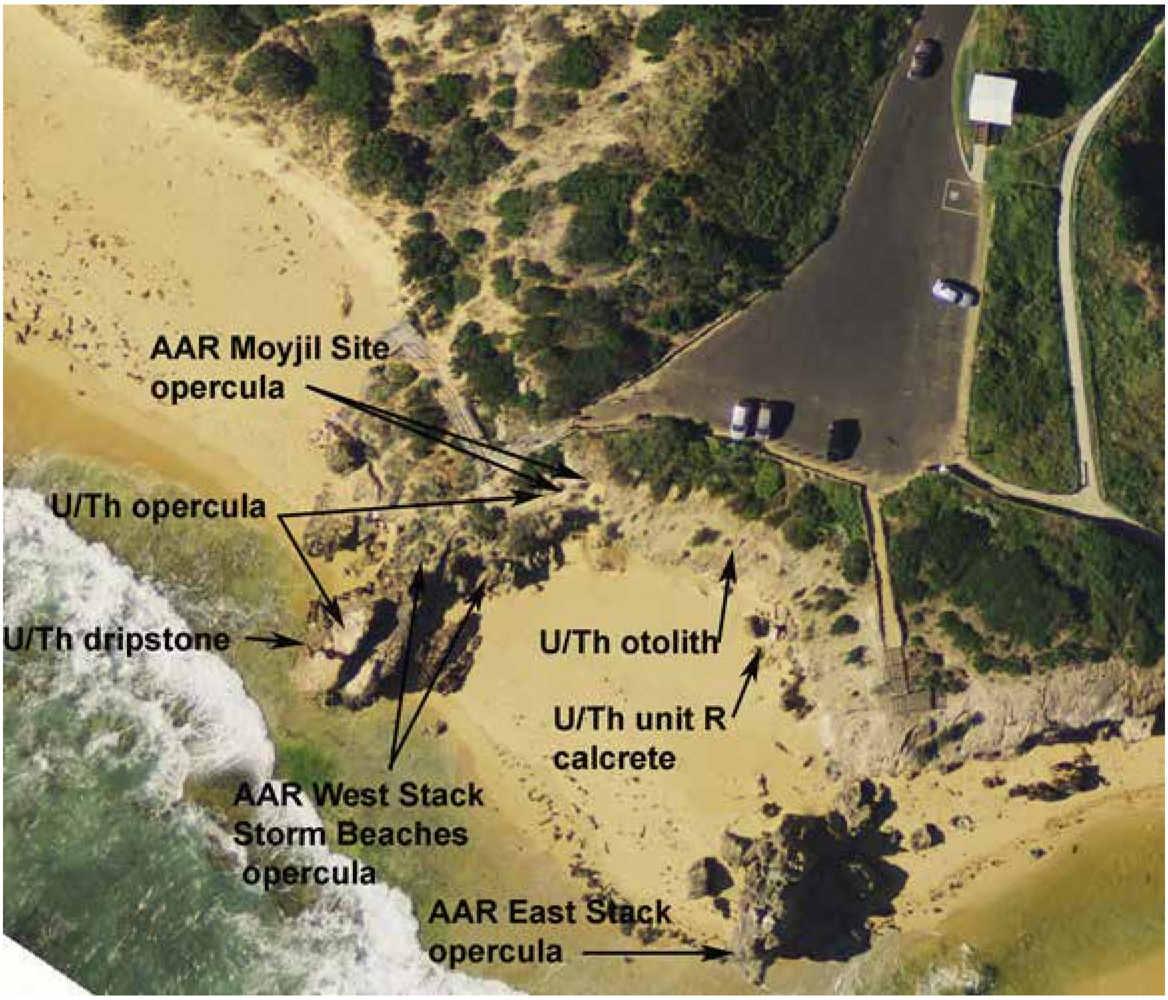

Figure 4: Location of samples collected for U/Th and AAR analyses. See text for details.

to define appropriate areas for geochemical analysis. The analytical system employs a Helex 193 nm laser ablation probe (see Woodhead et al. 2004) coupled to an Agilent 7700 quadrupole ICPMS. A spot size of 50 µm was used with a repetition rate of 5 Hz and laser power density of <5 $J.cm^{-2}$. NIST SRM 612 was used as the primary calibration material with calcium as internal standard. Data deconvolution employed the Iolite software package of Paton et al. (2011).

A detailed description of the U-Th analytical procedures is presented in Hellstrom (2003). In brief, separation of U and Th from carbonate samples was accomplished using Eichrom TRU ion-specific resin employing nitric, hydrochloric and hydrofluoric acid media. Isotope ratio determinations were performed on a Nu Plasma Multicollector ICPMS with sample introduction by a DSN100 desolvating nebuliser operating at an uptake rate of ~85 microlitres/minute.

Amino acid racemisation (AAR) dating

The ratio of D- to L-amino acids was determined for the opercula of fossil specimens of the marine mollusc *L. undulata* from five sites (Figure 4):

- Moyjil headland, recovered from unit Q2.
- A storm beach deposit (unit Q1) in a notch cut into East Stack ~2.5 m above present sea level (Sherwood et al. 1994).
- A storm beach deposit ~2.2 m above present sea level on the east side of West Stack (unit Q1).
- A storm beach deposit ~4.9 m above present sea level on the east side of West Stack (unit Q1).
- Goose Lagoon, a LIG deposit ~30 km west of Warrnambool (Sherwood et al. 1994).

Opercula of mature individuals (diameter 1.5–2.0 cm) were selected for analysis. The East and West Stack storm beach deposits (part of unit Q1) have not previously been dated by AAR.

The extent of amino acid racemisation (AAR) was determined for the slow and intermediate racemising amino acids, glutamic acid (GLU), leucine (LEU) and valine (VAL). The extent of racemisation was determined by reverse-phase, high-performance liquid chromatography (RP-HPLC). The analytical protocol followed that of Kaufman and Manley (1998). Following cleaning in an ultrasonic bath and an acid etch in 2M HCl to remove diagenetically modified outer portions of the shell carbonate and any surface-adhering sedimentary particles, the *Lunella* opercula were digested in 8M HCl and spiked with the internal standard L-*homo*-argenine (0.01M). Analyses were undertaken on the total hydrolysable amino acids after hydrolysis for 22 h at 110°C in 7M HCl. The analytical procedure involved the pre-column derivatisation of D/L-amino acids with *o*-phthaldialdehyde (OPA) together with the chiral thiol, *N*-isobutyryl-L-cysteine (IBLC) to yield fluorescent diastereomeric derivatives of the chiral primary amino acids. Amino acid D/L value determinations were undertaken using an Agilent 1100 HPLC with a C-18 column and auto-injector. Duplicate injections were completed for each operculum sample analysed.

Optically stimulated luminescence (OSL) dating

Previous work. Previous work using thermoluminescence techniques had been carried out at this site by Oyston (1996) and Sherwood et al. (1994). Subsequently, optical dating was applied by the late Professor J.R. Prescott (JRP) and F.M. Williams (FMW), but their data were not published. The results of Oyston and Sherwood et al.'s work are discussed below (see Results and Discussion). The unpublished OSL work undertaken by Prescott and Williams employed the same techniques as described below and yielded almost identical results. Re-sampling and re-analysis were undertaken in view of the perceived importance of the site in terms of possible human settlement. In particular, extremely rigorous measurements of the environmental dose rate were undertaken, which Prescott and Williams had shown to be very low and thus difficult to determine accurately. Only the results of the re-analysis by N.A. Spooner and D.G. Questiaux are presented here.

Sample collection. The site was designated as MR (from 'Moyjil–Ritchie'). The four samples were collected by N.A. Spooner, using stainless steel core cylinders hammered into a cleaned vertical face of the section. Three samples were taken from the western end of unit Q2 where it is thickest (~2 m) at locations near the base (MR3), centre (MR2), and top (MR1) of the sand layer. A fourth sand sample (MR4) was collected from mid-depth in a layer of intercalated sand and laminar calcrete (unit R).

Samples were selected based on the need to find sufficiently thick exposures of sediment to optimise the conditions for valid *in situ* gamma-ray dose determination, using a portable gamma-ray spectrometer, while avoiding disturbances caused by previous workers and natural erosional processes. Given the thinness of the unit Q2 sand layer, its three samples were spread laterally over approximately 10 m in order to prevent possible collapse of the section due to our activity. The location of each sample is shown in Figure 5.

In situ 'down hole' gamma-ray spectrometry was then performed at each sample location in order to measure the environmental dose rate experienced by the sample during its burial history. These measurements used a portable Ortec gamma-ray spectrometer with a 75 mm (3 inch) sodium iodide crystal. Bulk sediment samples were also collected from each sample location for additional

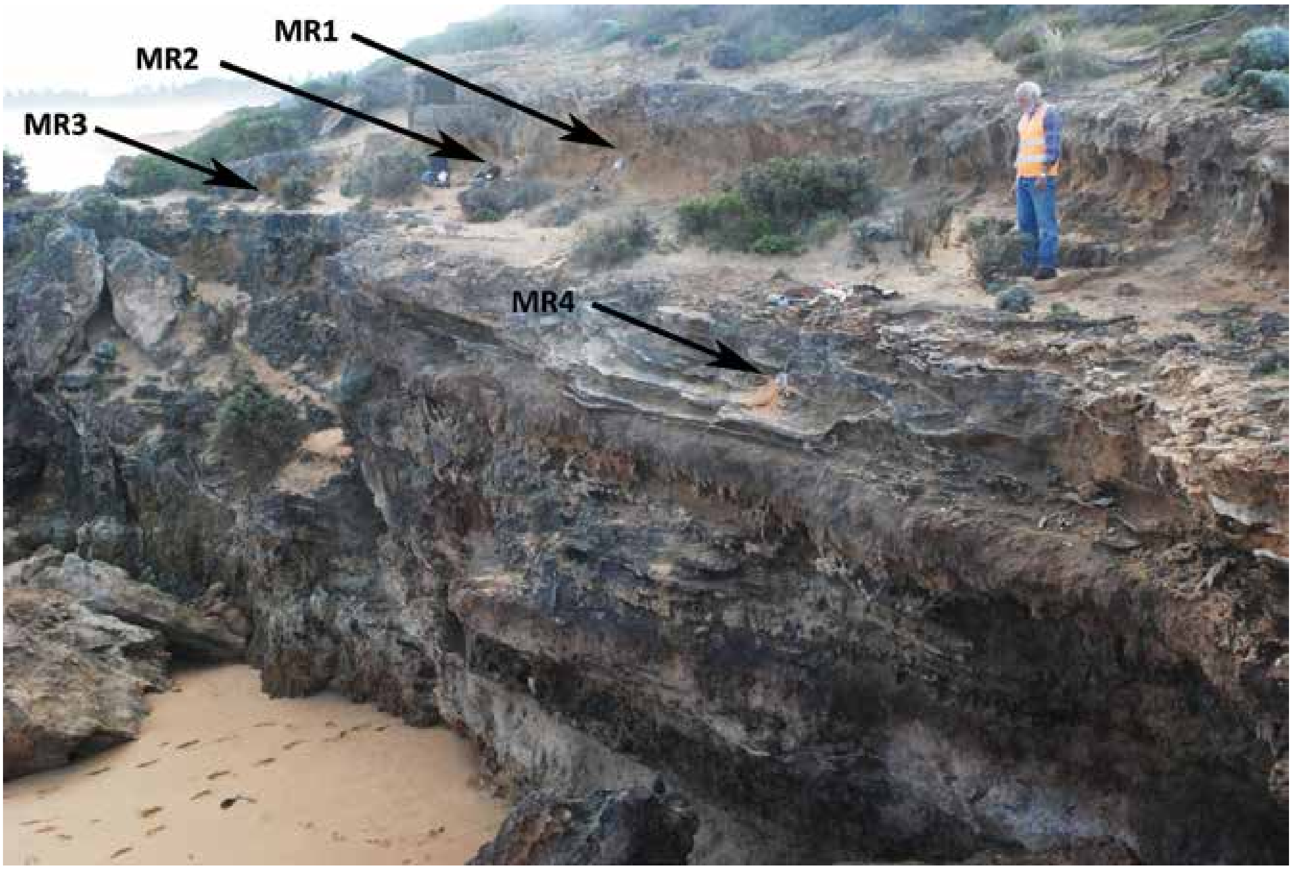

Figure 5: Location of OSL samples MR1 to MR4 (in order from highest to lowest elevation). Sherwood is standing on Ground surface alpha (above MR4 in unit R) with unit Q2 (MR1 – MR3) behind him. Photograph: N.A. Spooner.

laboratory radioisotope assay. These were taken from the material removed during the augering process.

Determination of environmental dose rates. The previous studies undertaken by JRP and FMW had shown that the total dose rate at this site was very low (~0.5 Gy/ka), challenging the detection limits of the methods applied. Our approach was guided by this experience and focused on techniques with very low detection limits and the ability to account for field dose-rate heterogeneity. The environmental dose rates were therefore measured both in the field using *in situ* gamma-ray spectrometry, and in the laboratory using inductively coupled plasma mass spectrometry (ICPMS) and X-ray fluorescence (XRF) to analyse concentrations of potassium, uranium and thorium. Laboratory high-resolution gamma-ray spectrometry was also undertaken in order to confirm that the nuclide decay chains were in radioactive equilibrium. Measurement procedures are given in detail elsewhere (Spooner & Questiaux 2015; Hamm et al. 2016). Nuclide concentrations, water content, gamma and cosmic ray contributions and calculated total dose rates are shown in Table 1.

Sediment water content (% dry weight) was measured at 125°C.The cosmic ray contribution was calculated from field measurements of overburden thickness, density, and assumed depositional history combined with the site's latitude, longitude, and altitude, using the relationships between cosmic ray flux, penetration, and geomagnetic position as determined by Prescott and Hutton (1994). Dose rates were calculated from the above data using the *Age* programme of Grün (2009). The calculated dose rates and the data used are shown in Table 1.

Sample preparation. Preparation followed the standard procedures applied in the PELL and described in Chen et al. (2002).

Luminescence measurements. All optically stimulated luminescence (OSL) measurements were carried out in the PELL using a Risø TL/OSL DA-20 reader. OSL was stimulated using a focused green laser diode (wavelength 532 nm) delivering sequential illumination to each of an array of 100 quartz grains per sample disc (grain diameter 231±19 μm). The emitted OSL was detected using an EMI 9235QB photomultiplier filtered by a 7 mm thick UV-transmitting Hoya U 340 optical filter. Laboratory irradiation was applied using a calibrated $^{90}Sr/^{90}Y$ β source mounted on-board the Risø TL/OSL DA-20 reader.

Four single-grain discs (100 grains) were prepared for each sample. For each sample, one disc was first analysed in a pilot study to determine the optimum radiation dose distribution for the luminescence measurement protocol.

Table 1: Field data, radionuclide concentrations and environmental dose-rates. The field gamma spectrometry data (ISGS) were used only for the gamma dose rates, and the mean HRGS, ICPMS or XRF data were used only for the beta and alpha dose-rate contributions. Abbreviations: asl – above sea level; ISGS – *in situ* gamma ray spectroscopy; HRGS – high resolution gamma ray spectroscopy; ICPMS – inductively coupled plasma mass spectroscopy; XRF – X-ray fluorescence.

Sample	**MR1**	**MR2**	**MR3**	**MR4**
Laboratory code	Ad14041	Ad14042	Ad14043	Ad14044
Stratigraphic unit	Q2	Q2	Q2	R
Burial depth (m)	1.2	1.6	2.2	2.5
Altitude (m asl)	9.5	9.0	8.5	8.0
H_2O content (% dry weight)	6 ± 2	7 ± 2	5 ± 2	10 ± 2
Nuclide concentrations				
K (%) (XRF)	0.05 ± 0.00	0.05 ± 0.00	0.03 ± 0.00	0.03 ± 0.00
K (%) (HRGS)	0.06 ± 0.00	0.06 ± 0.00	0.04 ± 0.00	0.04 ± 0.00
K (%) (ISGS)	0.06 ± 0.00	0.05 ± 0.00	0.04 ± 0.00	0.04 ± 0.00
U (ppm) (ICPMS)	1.00 ± 0.07	0.99 ± 0.07	1.04 ± 0.07	1.13 ± 0.07
U (ppm) (HRGS)	0.83 ± 0.01	0.94 ± 0.01	1.03 ± 0.01	1.13 ± 0.02
U (ppm) (ISGS)	0.80 ± 0.06	0.91 ± 0.07	0.97 ± 0.07	0.98 ± 0.08
Th (ppm) (ICPMS)	0.90 ± 0.06	0.94 ± 0.07	0.91 ± 0.07	0.92 ± 0.07
Th (ppm) (HRGS)	1.03 ± 0.02	1.13 ± 0.03	1.01 ± 0.02	1.14 ± 0.03
Th (ppm) (ISGS)	1.08 ± 0.09	0.99 ± 0.08	0.98 ± 0.08	1.02 ± 0.08
Cosmic ray contribution				
Cosmic ray dose (Gy/ka	0.18 ± 0.02	0.17 ± 0.02	0.16 ± 0.02	0.16 ± 0.02
Dose-rate components				
Internal alpha dose (Gy/ka)	0.013 ± 0.006	0.014 ± 0.007	0.015 ± 0.007	0.014 ± 0.007
Internal beta dose (Gy/ka)	0.003 ± 0.000	0.003 ± 0.000	0.003 ± 0.000	0.003 ± 0.000
External alpha dose (Gy/ka)	0.005 ± 0.003	0.005 ± 0.003	0.006 ± 0.003	0.005 ± 0.003
External beta dose (Gy/ka)	0.156 ± 0.009	0.153 ± 0.009	0.161 ± 0.009	0.152 ± 0.007
External gamma + cosmic dose (Gy/ka)	0.328 ± 0.020	0.323 ± 0.019	0.319 ± 0.019	0.310 ± 0.017
Total dose rate				
Total dose rate (Gy/ka)	0.51 ± 0.02	0.50 ± 0.02	0.50 ± 0.02	0.49 ± 0.02

The remaining discs were then measured using these optimised parameters in the Single Aliquot Regeneration (SAR) protocol devised by Murray and Wintle (2000). Six regeneration doses of values based on the pilot study and a zero dose were administered to each sample. Each irradiation-luminescence cycle was followed by a constant test dose to correct for sensitivity changes. Preheats used were those which had previously been confirmed as appropriate through a dose recovery test by JRP and FW in 2009: that is, 10 sec at 260°C for the doses and 160°C for test doses. This combination had given a dose recovery of 99.5 ± 1.5%. The zero dose cycle (used to establish the recuperation level) was followed by two repeats of the first dose cycle. In the first of these repeats, an infra-red (IR) shine was applied prior to the preheat and green OSL shine; in the second repeat, a green OSL shine only was applied. If the ratio of the luminescence measured for these final two dose cycles (termed the IR depletion ratio) was <0.15, the grain was rejected as being a feldspar. Feldspar luminescence is depleted by IR radiation, whereas that of quartz grains is not.

Grains having recycling of 85% or better, recuperation less than 15%, IR depletion ratio less than 15%, and reasonably smooth regeneration and test dose response curves were accepted for subsequent inclusion in the age analysis (27–34% for the four samples). Oversaturated grains (11–16%) and grains with no luminescence (19–24%) were necessarily rejected. A further 31–38% were rejected based on experimental criteria: low counts, bad growth curve, bad statistics, recuperation too high and supralinear growth curves.

RESULTS AND DISCUSSION

U-series dating

U–Th disequilibrium dating is dependent on two assumptions: first, that the sample did not contain detectible ^{230}Th at its time of formation; and second that it has remained a perfectly closed system with respect to U and Th since that time (Richards & Dorale 2003). Where the assumptions are met, ^{230}Th ingrowth proceeds as a function of U content, ^{234}U/^{238}U ratio and time, and allows calculation of numerical radiometric ages for samples of up to ~500,000 years (by which time ^{230}Th has closely approached secular equilibrium with its parent isotope ^{234}U).

The assumption of no initial ^{230}Th is true for pure calcite but breaks down where detrital material is incorporated. The presence of detrital material is tested by measuring ^{232}Th, which can only be found in a contaminating phase. Using an assumed initial ^{230}Th/^{232}Th ratio (and uncertainty) allows determination of the ^{230}Th content at the time of formation and thus a corrected age and its uncertainty (Hellstrom 2006). The closed-system assumption is usually true for crystalline calcite precipitated from groundwater, but can be tested using repeat analyses of different portions of a sample: if the apparent ages of three or more samples are equivalent with respect to their uncertainties then it is considered likely that the sample behaved as a closed system.

U–Th analyses (Table 2) were applied to three replicate samples of both the thin (*ca* 15 mm) calcite dripstone layer (A1–A3) and the calcrete (B1–B3); duplicate analyses were made on the two *Lunella* opercula (C1–C2; D1–D2); and five replicates were analysed for the otolith (E1–E5).

The West Stack notch dripstone returned robust ages of 14.1 ± 0.1, 11.0 ± 0.1, and 10.8 ± 0.2 ka (Samples A1–A3 in Table 2) indicating it grew predominantly during the late Last Glacial and/or early Holocene.

Calcrete is usually difficult or impossible to date using U-Th due to very high detrital sediment content (Branca et al. 2005; Candy et al. 2004; Kelly et al. 2000) but in this case ^{230}Th corrections were less than 4% of the sample age (Samples B1–B3 in Table 2), returning three indistinguishable and thus reliable ages of ~103.5 ka. The calcrete occurs within cemented sand dated to 239 ka using OSL (sample MR4) with relatively sharp contacts between. This suggests much later post-depositional precipitation of the calcite within the sand, probably via groundwater.

Whilst U–Th dating of molluscan shells has been attempted in the past with little success due to open-system behaviour (Hillaire-Marcel et al. 1996; Kaufman et al. 1971), opercula have been found to better approximate closed geochemical systems (Penkman et al. 2013). Fish otoliths have previously been shown to give incorrect U-Th ages (Herczeg & Chapman 1991) but this could be due to uptake close to the sample surface. To assess the likelihood of post-depositional open-system behaviour, the two *Lunella* opercula and the fish otolith were scanned using spatially resolved laser-ablation inductively-coupled plasma mass spectrometry (Woodhead et al. 2007, 2008) to determine the internal distribution of U and Th. As expected, their outer surfaces appeared to be heavily contaminated by post-depositional U and Th uptake but they also exhibited low levels (tens of ppb or less) internally suggesting limited uptake or mobility there and justifying an attempt at U-Th dating. A number of internal samples of ~1 mg were obtained for geochronology by micro-drilling.

Unfortunately, none of these analyses proved successful. The two operculum samples returned apparent ages ranging from 92 to 132 ka (Table 2; samples C and D) and cannot be considered reliable due to uranium mobility, as is typically observed for molluscan shells. Five independent zones of the otolith were sampled and analysed, resulting in a spread of apparent ages (Table 2; samples E1–E5) from 108 to 162 ka which also indicates post-depositional U mobility. High levels of Th measured in the core of the otolith are unlikely to have been present during the life of the fish and are also interpreted as post-depositional in nature. The operculum and otolith results thus do not permit the calculation of true ages and therefore place no constraints on sample age.

Amino acid racemisation (AAR) dating

Amino acid D/L values for glutamic acid (GLU), leucine (LEU), and valine (VAL) in *L. undulata* opercula are shown in Table 3. D/L values reported here are mostly higher than for corresponding sites reported in Sherwood et al. (1994; Table 3). For the Moyjil site the present values are about twice those of Sherwood et al. (1994). This is considered

Table 2: U–Th activity ratios and ages determined using a Nu Plasma MC-ICP-MS at the University of Melbourne. 2σ uncertainties in brackets are of the last two significant figures presented except for age which is absolute.

Sample	U(ng.g^{-1})	[^{230}Th/^{238}U][a]	[^{234}U/^{238}U][a]	[^{232}Th/^{238}U]	[^{230}Th/^{232}Th	Age (ka)[b]	[^{234}U/^{238}U]$_i$[c]
Drip Stone-A1	197	0.1275 (11)	1.0482 (29)	0.0000863 (21)	1477	14.14 (0.14)	1.0502 (30)
Drip Stone-A2	146	0.10141 (56)	1.0526 (30)	0.0002445 (27)	415	11.026 (0.077)	1.0543 (31)
Drip Stone-A3	100	0.1020 (16)	1.0659 (48)	0.001557 (19)	65.5	10.81 (0.21)	1.0679 (50)
Unit R Calcrete-B1	179	0.7249 (32)	1.1372 (28)	0.04806 (78)	15.1	103.1 (2.5)	1.1836 (37)
Unit R Calcrete-B2	180	0.7210 (28)	1.1336 (28)	0.04330 (54)	16.7	103.2 (2.3)	1.1789 (37)
Unit R Calcrete-B3	180	0.7236 (29)	1.1312 (26)	0.04168 (41)	17.4	104.4 (2.2)	1.1762 (34)
Unit Q2 Operculum1-C1		0.837 (23)	1.1480 (98)	0.0535 (17)	15.6	131.6 (8.0)	1.215 (13)
Unit Q2 Operculum1-C2		0.911 (39)	1.174 (15)	0.2389 (82)	3.81	130 (19)	1.252 (23)
Unit Q2 Operculum2-D1		0.757 (19)	1.247 (11)	0.0724 (16)	10.4	91.7 (5.2)	1.320 (14)
Unit Q2 Operculum2-D2		0.932 (35)	1.285 (22)	0.02524 (49)	36.9	129 (10)	1.411 (28)
Unit Q2 Otolith-E1		0.787 (18)	1.202 (20)	0.04412 (86)	17.8	107.5 (5.9)	1.273 (25)
Unit Q2 Otolith-E2		0.895 (23)	1.199 (12)	0.01870 (32)	47.9	139.7 (7.8)	1.295 (17)
Unit Q2 Otolith-E3		0.927 (22)	1.179 (12)	0.01558 (31)	59.5	156.2 (9.0)	1.278 (17)
Unit Q2 Otolith-E4		0.807 (40)	1.180 (15)	0.0314 (13)	25.7	118 (11)	1.252 (20)
Unit Q2 Otolith-E5		1.037 (69)	1.261 (18)	0.1053 (27)	9.85	162 (26)	1.412 (37)

a Activity ratios determined after Hellstrom (2003) using the decay constants of Cheng et al. (2013).
b Age in ka before present corrected for initial ^{230}Th using eqn. 1 of Hellstrom (2006) and initial [^{230}Th/^{232}Th] of 1.0 ± 0.5.
c Initial [^{234}U/^{238}U] calculated using corrected age.

to be due to the different digestion and chromatographic techniques applied. The Goose Lagoon site, however, differs in that values in the two studies are the same, an apparently anomalous result with important ramifications for interpretation of the age of the Moyjil site.

The Moyjil storm-beach deposits have not previously been studied by the AAR technique. D/L values for the three deposits analysed are closely grouped for all three amino acids. Given their close geographical association and therefore comparable diagenetic temperature histories, the similar extent of racemisation in each indicates that the shells are of equivalent age (Table 3). The shells are correlated with the LIG maximum (MIS 5e) based on the extent of AAR corresponding with other MIS 5e successions in southern Australia (Murray-Wallace et al. 2010). The elevation of the sedimentary succession at 2–6 m AHD and its location are also consistent with a LIG age (Hearty et al. 2007; Murray-Wallace & Woodroffe 2014; Murray-Wallace et al. 2016). ESR studies of two of the storm-beach deposits (one on East Stack and one ~70

Table 3. Extent of amino acid racemisation in opercula of *Lunella undulata* (syn. *Turbo undulatus*) from Moyjil and a reference Last Interglacial site (Goose Lagoon) 30 km to the west (Sherwood et al. 1994).

Location	N	Laboratory Codes UWGA-	GLU	LEU	VAL	Source
Goose Lagoon (LIG)	9 (4)*	10,101	0.29 ± 0.04	(0.32 ± 0.04)*	0.20 ± 0.04	this study
Moyjil Site (unit Q2)	4	9744, 9968, 9969	0.32 ± 0.05	0.34 ± 0.08	0.24 ± 0.06	this study
Unit Q1 Storm beach, East Stack#	2	9745	0.406 ± 0.006	0.44 ± 0.02	0.336 ± 0.004	this study
Unit Q1 Storm beach, West Stack 4.9 m AHD#	4	9970, 9971, 9746	0.39 ± 0.02	0.43 ± 0.05	0.31 ± 0.04	this study
Unit Q1 Storm beach, West Stack 2 m AHD#	4	9747, 9972, 9973,	0.36 ± 0.02	0.41 ± 0.03	0.295 ± 0.008	this study
Goose Lagoon (LIG)	2 (3)*		0.29 ± 0.01	0.26 ± 0.01	(0.20 ± 0.04)*	Sherwood et al. (1994)
Moyjil Site (unit Q2)	6		0.17 ± 0.05	0.17 ± 0.05	0.11 ± 0.04	Sherwood et al. (1994)

* Number of samples in parentheses applies to the ratios given in parentheses for particular amino acids.

Table 4: Maximum and minimum racemisation values found for *Lunella undulata* (syn. *Turbo undulatus*) from Goose Lagoon, Moyjil's unit Q2 and the three (combined) Moyjil storm beach (unit Q1) deposits in the present study.

Location	N	GLU	LEU	VAL
Goose Lagoon	9 (4)*	0.25 - 0.37	(0.29 – 0.38)	0.16 – 0.28
Moyjil unit Q2	4	0.27 – 0.39	0.28 – 0.45	0.20 – 0.33
All Moyjil Storm beaches (unit Q1)	10	0.34 – 0.41	0.36 – 0.47	0.25 – 0.35

* Number of samples in parentheses applies to the D/L value for leucine.

m NE of it on the bank of the Hopkins estuary) place them in the same resonance zone as the LIG Goose Lagoon site (Goede 1989).

Mean D/L values for the three amino acids are the same for Goose Lagoon and the Moyjil site, contradicting findings of Sherwood et al. (1994). The three amino acids in the present study (GLU, LEU and VAL) were among eight analysed for the 1994 paper. In that paper all eight amino acids gave ratios in the same relative order, i.e. Modern < Moyjil < Goose Lagoon. Other evidence supported a LIG (125 ka) age for Goose Lagoon and so Moyjil was taken to be younger than this. We are unable to explain this change in ordering of the two sites, although it is possible that relatively small sample sizes (N < 4) have biased some ratios.

At Moyjil, differences in environmental factors would be expected to be small for deposits of similar age, giving greater confidence with inter-site comparisons. The Moyjil site (unit Q2) has lower mean D/L values than the Moyjil storm beaches (unit Q1) but these mostly overlap at the 1σ level, except for GLU and VAL ratios of the East Stack deposit. This and the large scatter in individual ratios are such that the datasets must be considered to overlap (Table 4). The main objective of the present AAR study was to investigate the age of the Moyjil site compared with that of the Moyjil and Goose Lagoon LIG natural shell beds.

They are the same age within the resolution of the AAR method, which is not sufficient to distinguish ages between the beginning (MIS 5e) and the end (MIS 5a) of the LIG *sensu lato*.

Analysis of the luminescence measurements

In Figure 6, the measured D_es of the individual accepted grains for each sample are presented as Abanico plots (Dietze et al. 2016).

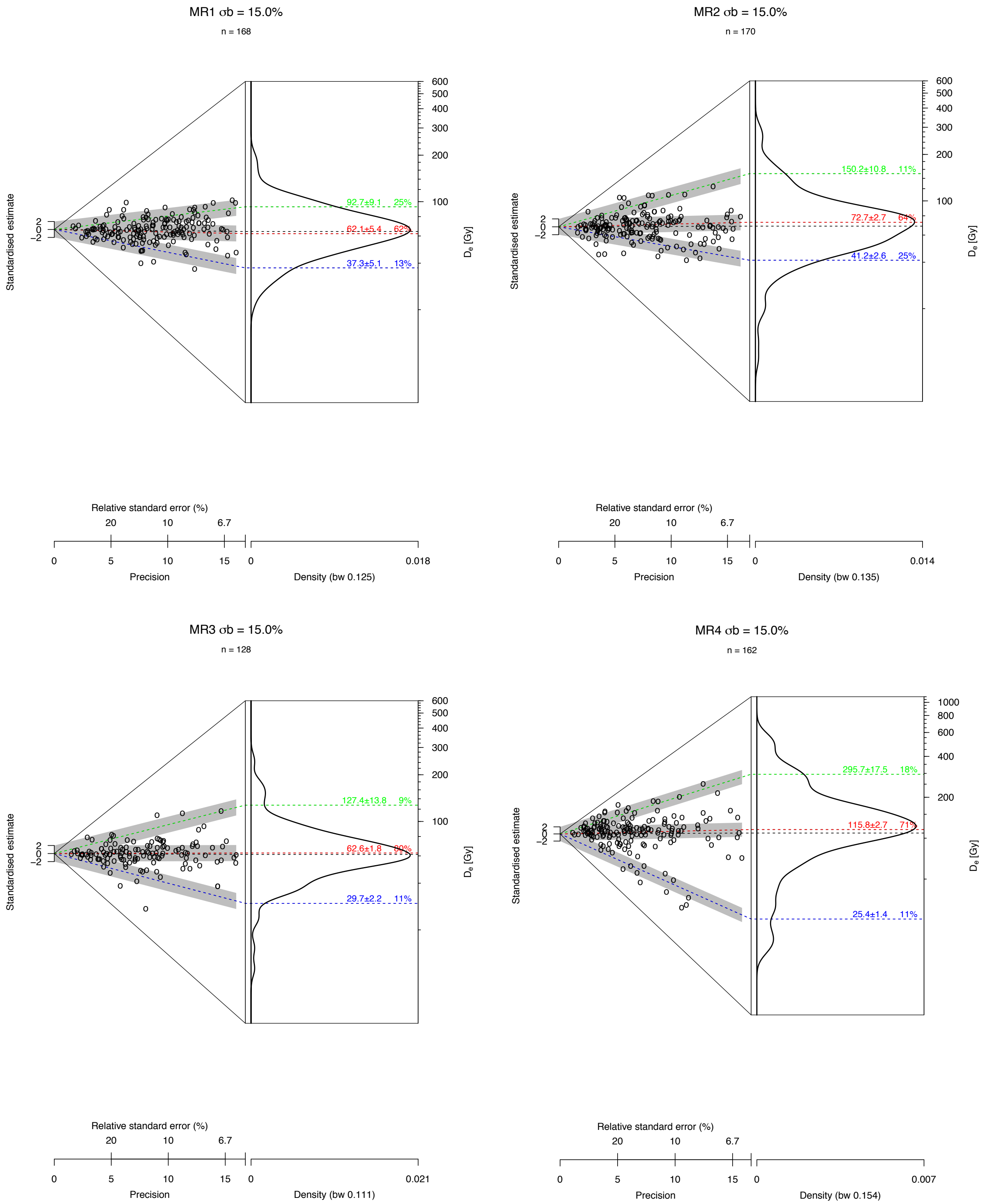

Figure 6: Abanico plots for samples MR1, MR2, MR3 and MR4, based on a three-component Fmix population model. The three predicted mean values of ED for each sample (shown in colour on each figure) are listed in Table 5.

Overdispersion. All the samples showed overdispersion much greater than was obtained with the dose response tests, and much higher than 15–20%. That is, more than 5% of D_e values lie outside the 2σ range defined by the measurement uncertainty (Lian & Roberts 2006; Pietsch 2009; Jacobs et al. 2006). The overdispersion ranged from 28–68%, compared with the dose recovery test, which showed an overdispersion of 13.8%. Jacobs et al. (2006) listed the possible causes of overdispersion. In the case of the Moyjil samples, beta-dose heterogeneity would have a negligible effect since the major contribution to the environmental dose is from external gamma and cosmic rays (see Table 1). Incomplete bleaching before burial normally results in a skewed distribution of D_e, with a long tail toward higher values. Such is not observed in this case. The D_e distribution for each of the Moyjil samples was broad but with a noticeable tendency to cluster within certain ranges of values, one range in general being dominant (see Figure 6). The samples from unit Q2 each show a dominant age component, generally consistent with early MIS 5 deposition, accompanied by vertical or lateral mixing of material over an extended period of time. Possible mechanisms for this scenario will be presented below. Sample MR4 (unit R) shows a clear dominant component of age of about 240 ka (MIS 7), with some mixing of younger material from the 50–60 ka period prior to the development of the sealing calcrete, and also of mixing from the underlying older unit.

Modelling the grain populations. Three statistical models are commonly used for the interpretation of D_e datasets: the Minimum Age Model (MAM) (Galbraith et al. 1999), the Central Age Model (CAM) (Galbraith et al. 1999) and the Finite Mixture Model (Fmix) (Galbraith & Green 1990). MAM is applicable to a deposit in which only a small proportion of grains have been fully bleached. Here it was determined to be inapplicable as explained above. CAM is generally applied to datasets which do not have a large overdispersion (typically less that about 15%), implying a deposit consisting of fully bleached grains emplaced within a distinct period of time, and for which the individual D_e values can, in effect, be averaged. The D_e distribution is typically of near-symmetrical 'Gaussian' type with a single peak. The distributions observed for the four samples here are broadly Gaussian in form, and hence we have applied the CAM as an indicative assessment and include the results in Table 5.

Fmix is ideally applicable to a distribution which has a number of discrete populations. It distinguishes each population, or component, and determines the central value of each. However, it may also be applied with caution to a continuum of values with less well-defined groupings of individual values, as is the case for the Moyjil samples, and this model was therefore selected for the analyses. Three-component Fmix fits (Fmix3) were used for all four samples, based on the Bayesian Information Criterion (Schwarz 1978) and maximum likelihood analysis, and

Table 5: Equivalent doses, dose rates and ages of unit Q2 (MR1 – MR3) and unit R (MR4) sands calculated using both CAM and three-component Fmix approaches.

Sample (depth (m))	Dose rate (Gy)	Fit model	Overdispersion (%)	Proportion of grains (%)	Equivalent dose (Gy)	Age (ka)
					(Uncertainty 1σ)	
unit Q2 MR1 (1.2m)	0.51 ± 0.02	CAM	28	100	64.1 ± 1.7	126.7 ± 6.9
		Fmix		13	37.3 ± 5.1	73.7 ± 10.7
		Fmix		62	62.1 ± 5.4	122.7 ± 12.2
		Fmix		25	92.7 ± 9.1	183.3 ± 19.6
unit Q2 MR2 (1.6m)	0.50 ± 0.02	CAM	41	100	67.9 ± 2.5	136 ± 8
		Fmix		25	41.2 ± 2.8	82.6 ± 6.8
		Fmix		64	72.7 ± 2.7	145.7 ± 8.6
		Fmix		11	150.2 ± 10.8	301 ± 26
unit Q2 MR3 (2.2m)	0.50 ± 0.02	CAM	38	100	61.0 ± 2.3	121.0 ± 7.2
		Fmix		11	29.7 ± 2.2	58.9 ± 5.1
		Fmix		80	62.8 ± 1.8	124.6 ± 6.7
		Fmix		9	127.4 ± 13.8	253 ± 30
unit R MR4 (2.5m)	0.49 ± 0.02	CAM	68	100	115.7 ± 6.6	239 ± 17
		Fmix		11	25.4 ± 1.4	52.4 ± 3.7
		Fmix		71	115.8 ± 2.7	239 ± 12
		Fmix		18	295.7 ± 17.5	610 ± 45

the central value for each population was determined. It is important to note, however, that these values do not necessarily define discrete populations, but indicate maxima in the distribution.

The values of D_e used in the age calculation and the corresponding ages are shown in Table 5. The ages are calculated by dividing D_e by the corresponding dose rate. Comments on individual samples are given below:

(a) Unit Q2

All three samples showed similar results — a dominant population (62–80%) of LIG grains (122–146 ka) with smaller proportions of both younger (59–83 ka) and older grains (183–301 ka)

- MR1. This sample had a main population grouping of measurable grains (62%) with a central value of 123±12 ka. The next largest group (25%) had a population centred on 183±20 ka. This is interpreted as showing two depositional phases, the second of which peaked at 123±12 ka and resulted in major mixing with a pre-existing 183±20 ka deposit. This earlier deposit is most likely the unit R sand, deposited in Marine Isotope Stage (MIS 7) but it could also represent a younger aeolian deposit.

  A third distinct, but smaller population (13% of measurable grains) had an age of 74±11 ka. The much smaller fraction of the total sediment mass represented by this population and the clearly younger age led to the interpretation that these grains represent a post-depositional event, possibly bioturbation by plant roots or burrowing animals, which mixed this younger material downwards into the existing sand body. It is probable that the mixing event, or series of events, took place before the formation of the overlying calcrete. The age of 74±11 ka could therefore also be inferred as indicating the time at which the calcrete effectively became impervious.
- MR2. This sample showed a broad distribution of D_e with the principal population (64% of the measurable grains) centred at 146±9 ka, and a significantly younger population (25%) at 83±7 ka. The three-component fit also revealed a small population (11% of measurable grains) of much older grains of 301±26 ka. This is likely reflecting the intrusion of these more ancient grains from the underlying unit.
- MR3. This sample also showed a wide range of D_e, but Fmix3 found that the majority (80%) were centred at 125±7 ka, corresponding to Marine Isotope Stage 5e (MIS 5e; 120–125 ka). The remaining two components (centred at 59±5 ka and 253±30 ka) were present in almost equal proportions. The younger population is noted to be overlapping at 1σ with the youngest 13% of the MR1 sample. The oldest component (9% of the measurable grains) has a much greater age, 253±30 ka, which may correspond to deposition in MIS 7. The presence of this older grain population is attributed to grain mixing from unit R.

(b) Unit R

- MR4. This sample was collected from close to (within ~50 cm) but beneath the calcrete floor (unit Rcp) of unit Q2. The Fmix3 analysis revealed most of the sediment (70% of measurable grains) to be ~239±12 ka, in close agreement with the age of the oldest component measured in MR3 and supporting the conjecture that there was mixing of older material into the overlying MR3 sample, with unit R being the source. There is also a significant component of grains of age 52±4 ka which must have intruded from overlying units. Finally, a substantial proportion (18%) of the datable grains is of much greater age, ~610±45 ka. This age is interpreted as being that of the surface unit existing at the time of deposition of the 240 ka unit, with the 18% subsequently becoming mixed into the new, overlying material. This interpretation suggests that at this location, at least, there was a substantial depositional hiatus, or erosive event(s) between 240 and 600 ka.

Discussion of the OSL ages of unit Q2 and unit R sands. Although the data are resolved by Fmix3 into three components for each sample from unit Q2, we also note that on combining results for these three samples a significant proportion of the grains (47%) fall within an age range which spans MIS 5e (120–125 ka). The CAM values also agree in each case with a major LIG component of Fmix3 — a logical result if the sand body was deposited in a reasonable time frame (i.e. a few thousand years). An interpretation in which the sand was deposited during early MIS 5 but with a major component of the total material (15%) corresponding to an older depositional phase could account for this: the older material could be derived from a terrestrial aeolian or reworked marine sand deposited at 150–180 ka. Alternatively, and more likely, this population could represent a contribution from slow downslope movement of continually reworked MIS 7 sands. The large Dennington dune (>30 m AHD) currently lies immediately north of the Moyjil headland (Figure 1). Its size, location and degree of cementation are consistent with a LIG (MIS 5) age. It is likely, however, that the LIG sand is a drape over an earlier dune at this location since there are two thick (up to ~0.5 m) calcretes on the dune, the upper calcrete (Q2cs) being post-MIS 5 and the lower one (Rcs) post-MIS 7. There is evidence for downslope sand movement on some of the quartz grains themselves. Microscopic examination of quartz grains from a basal grey sediment in unit Q2 reveals reddish cutanic clay coatings on them, consistent with their derivation from a pre-existing soil. Higher in unit Q2 the grains show the clean surfaces expected of marine-derived windblown sands.

At the peak of the LIG (~120–125 ka; Lambeck & Chappell 2001; Hearty et al. 2007) we believe that sea level would have been sufficient (~8 m) to sweep the unit R calcrete surface (Gsα; Carey et al. 2018) clean of poorly consolidated sediment. The timing of reburial of the platform would thus be after this sea-level peak and as a falling sea exposed offshore sediment. Sand from two distinct populations was subsequently deposited on the platform. The age of one population is consistent with a major depositional phase at MIS 5e (120–125 ka; 62% of MR1, 80% of MR3) along with significant components dating to late MIS 5a-5c (mean age 83 ka; 25% of MR2), likely reflecting bioturbation of the MIS 5e material. A second population (>145 ka; 25% of MR1, 75% of MR2, 9% of MR3) represents older sand introduced laterally or from below by slumping or other turbation processes. It is also possible that the 64% of material in MR2 dating to about 145 ka also derives from MIS 5e as the 2σ ranges for the dominant fractions of the three samples (MR1-3) show substantial overlap. It may be that they represent a single population, most likely resulting from deposition after the MIS 5e high sea level, and the younger populations within them may reflect post-depositional bleaching caused by an unidentified diagenetic process; that is, the older population represents the depositional age of the sand on Gsα (i.e. post ~120–125 ka).

Irrespective of the depositional process, the wide range of ages found in each sample indicates considerable mixing of the material during and following deposition. Lying near the toe of a large dune, its environment is likely to be one of disturbance. The massive and uniform nature of the thin unit and the absence of stratification are consistent with a reworked and mixed deposit. How the mixing occurred is a matter for conjecture, but mass movement from upslope or some kind of bioturbation seem likely. Rhizomorphs show that roots penetrated the deposit, and there is evidence of some animal burrows as voids within the sand. One very likely candidate for bioturbation is the activity of ants, which can burrow extensively through 2 m and more of soil or fine sand (e.g. Paton et al. 1995) leaving little physical trace. Incorporation of sand from above would have been possible for only a limited amount of time. Once the upper calcrete developed, unit Q2 would have been effectively sealed above and below.

Unit R has an age close to MIS 7 (~180–245 ka) and may be a remnant aeolian deposit from that interval of higher sea level. Over 8 m of older calcarenite and palaeosols underlie this deposit and upward movement of sands from these beds could have introduced the older grains detected. Alternatively, downslope movement of sand from a former older dune could also have contributed incompletely bleached sands.

Comparison of OSL and TL studies. The unit Q2 sand has been investigated previously by TL (JRP in Sherwood et al. 1994; Oyston 1996). Oyston's PhD thesis included a detailed study of the calcarenite of the Warrnambool region, and at Moyjil he investigated unit Q2 and sedimentary units below it (units R, S, T and V). The heterogeneous nature of the Q2 sands implies batch techniques as used by Prescott and Oyston are unlikely to produce reliable ages for it. Using the lower dose rates measured here and their measured D_es for unit Q2 increases their calculated ages to 80–100 ka — still lower than found here. Additionally, Oyston's ages for units below unit Q2 are too young based on stratigraphic grounds and the OSL age for unit R (Carey et al. 2018).

SUMMARY OF FINDINGS BY ALL METHODS

Carey et al. (2018) have described the geological events which place definitive stratigraphic controls on the age of the various units of Moyjil headland. Unit R sands lie on top of an 8 m cliff in a bay facing the open ocean. Units below this (units S, T, and V) are calcarenite/palaeosol couplets that have resisted marine erosion during past intervals of higher sea level. Based on the OSL age for unit R (~240 ka) these units must be considerably older than their previously reported TL ages (Sherwood et al. 1994; Oyston 1996).

Wave-cut notches in the cliff below unit R have previously been assigned to the LIG (Goede 1989; Sherwood et al. 1994), a conclusion now confirmed by the AAR analyses of the present study. While most of the notches are at 3–4 m AHD the highest of these, located horizontally ~6 m from the cliff face, is at 6 m AHD. Gill and Amin (1975) reported a LIG sea level of 7.5 m AHD near Warrnambool. Such high seas would have resulted in strong marine erosion on the surface of unit R. It is hard to see how the sand of unit R could survive such erosion without a calcrete capping.

The central focus of the present and earlier studies at Moyjil has been to refine an age estimate for the shell-bearing sediment identified as unit Q2 in Carey et al. (2018). Both OSL and AAR agree on a LIG age *sensu lato* for unit Q2, older than previously reported (Sherwood et al. 1994) and with OSL suggesting a MIS 5e age. Stratigraphic considerations allow further refinement of that estimate. The MIS 5e high sea level at 120–125 ka swept the unit Rcp calcrete surface clean, allowing shells and discoloured (burnt?) stones to accumulate on a bare rock surface (identified as Gsα; Carey et al. 2018) as the sea retreated.

Subsequently, newly exposed shoreline sands were blown over Gsα and mixed with an almost equal volume of older sand — either from upslope or from below — and the unit Q2 layer was formed, burying the LIG beach and West Stack. As unit Q2 was deposited, occasional shells and rarer discoloured pebbles were incorporated in it.

During or after the burial process, groundwater penetrated unit R forming a calcrete (~103 ka by U-Th). A soil developed on unit Q2 and an associated calcrete formed until (by OSL modelling) it became a seal on the underlying sand at ~60 ka, precluding any further bioturbation. Erosion stripped the overlying *terra rossa* and at 35±3 ka a blanket of Tower Hill ash covered the surface. Erosion and/or weathering has removed evidence of the tuff and underlying *terra rossa* from all but the eastern side of the headland. The upper layers of Moyjil are formed by a stiff dark soil derived from the tuff and/or unidentified later sediments and overlying Holocene sands.

One other feature has been dated by U–Th in this study. Dripstone coated the surface of a sand which almost completely fills a LIG notch on West Stack some time during 11–14 ka. Formation of the dripstone suggests more restricted air circulation in the notch than presently exists. Higher sea level since ~7 ka has resulted in the stripping of material that formerly enclosed the notch, most likely the LIG unit Q1 deposit which surrounded the stack or the unit Q2 drape. Fragmentary remnants of the LIG beach remain in notches at multiple locations around the Moyjil headland.

Sometime after 11 ka (based on U–Th dating of dripstone) the prominent West Stack broke into four large pieces, two falling to the west and two to the east. That this may have happened within the last one hundred years is suggested by a 1907 postcard which appears to show an unbroken West Stack with a horizontal upper surface.

Age and shell bed origin

The relationship between the position of the sea and the time of formation of the site has been discussed in Nair and Sherwood (2007). There were three main sea-level peaks during the LIG: at ~120–125 ka, ~110 ka, and ~80 ka (Lambeck & Chappell 2001; Hearty et al. 2007). The presence of marine shells shows the coast was nearby at the time of deposition of unit Q2. If the shelly deposit is a seabird midden then the coast must have been very close to Moyjil since seabirds are unlikely to transport shells more than a few hundred metres inland. A seabird origin would imply an age close to the LIG sea-level maximum (120–125 ka). Humans are reported to transport subsistence-related marine shells many kilometres from the coast. For example, Aboriginal middens with *Lunella* and 'other reef gastropods' shells have been recorded up to 16 km inland in South Australia (Luebbers 1978: 105). Similarly, late Pleistocene sites along the coast of Portugal reveal exploitation of marine shellfish from sites located 10–20 km inland (Haws et al. 2011: 238). The requirement for a coast in close proximity to Moyjil is considerably relaxed for a human origin. Sea level was ~25 m below present level at 80 ka (Lambeck & Chappell 2001). Based on the present seafloor bathymetry (and ignoring any sand deposition or erosion by advancing and retreating seas) this implies a coast ~4 km off the modern shore (Figure 7). The 110 ka peak was slightly higher (~20 m below present) and the coast slightly closer than at 80 ka. Deposition of unit Q2 appears to have followed closely after the MIS 5e sea-level maximum and indicates deposition of shell material took place close to the coast of the time. As a consequence, neither origin (i.e. seabird or human) can be ruled out.

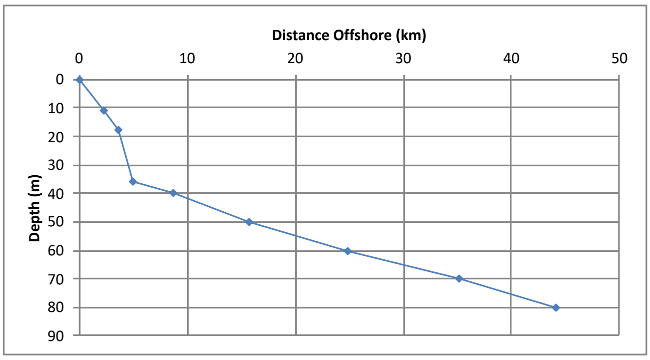

Figure 7: Bathymetry directly south of Moyjil. Source: AHS, 1965.

CONCLUSIONS

The unit Q2 sands are LIG in age as determined by both AAR of *Lunella undulata* (syn. *Turbo undulatus*) opercula and OSL of their host sand. This age is significantly older than previously determined (Sherwood et al. 1994). Unit Q2 has had a complex history, but a significant fraction of the single-quartz grain OSL ages points to an early LIG age (120–125 ka). Sands from unit R stratigraphically below unit Q2 are dated by OSL to be 240 ka (i.e. MIS 7). The unit Q1 deposits preserved at Moyjil between 2 and 6 m AHD are remnants of a MIS-5e beach. Deposition of unit Q2 is most likely to have occurred relatively soon after the MIS 5e sea-level maximum and in close proximity to the coast of the time.

Acknowledgements

At our request, Professor Jon Olley, Professor Bert Roberts and Professor Martin Williams informally reviewed the progress of Professor Prescott's incomplete OSL research on Moyjil after his death. Their comments and suggestions contributed to the results reported here.

Funds for the OSL analysis were provided from an Australian Government Indigenous Heritage Programme Grant to Warrnambool City Council.

The Eastern Maar Aboriginal Corporation, Gunditj Mirring Traditional Owners Aboriginal Corporation and Kuuyang Maar Aboriginal Corporation have supported research at Moyjil, as have Aboriginal Victoria and the Warrnambool City Council.

References

AHS, 1965. *1: 150,000 Bathymetric Survey Map Cape Nelson to Lady Bay*. Australian Hydrographic Service. Commonwealth of Australia.

Branca, M., Masi, U. & Voltaggio, M., 2005. An unsuccessful attempt at U-Th dating of soil calcretes from the Doukkâli area (western Morocco) and environmental implications. *Chemie der Erde - Geochemistry* 65: 347–356.

Candy, I., Black, S. & Sellwood, B.W., 2004. Quantifying time scales of pedogenic calcrete formation using U-series disequilibria. *Sedimentary Geology* 170: 177–187.

Carey, S.P., Sherwood, J.E., Kay, M., McNiven, I.J. & Bowler J.M., 2018. The Moyjil site, south-west Victoria, Australia: stratigraphic and geomorphic context. *Proceedings of the Royal Society of Victoria*, this volume.

Chen, X.Y., Spooner, N.A., Olley, J.M. & Questiaux, D.G., 2002. Addition of aeolian dusts to soils in southeastern Australia: red silty clay trapped in dunes bordering Murrumbidgee River in the Wagga Wagga region. *Catena* 47(1): 1–27.

Cheng, H., Lawrence Edwards, R., Shen, C.-C., Polyak, V.J., Asmerom, Y., Woodhead, J.D., Hellstrom, J., Wang, Y., Kong, X., Spötl, C., Wang, X. & Alexander, E.C., Jr, 2013. Improvements in ^{230}Th dating, ^{230}Th and ^{234}U half-life values, and U–Th isotopic measurements by multi-collector inductively coupled plasma mass spectrometry. *Earth and Planetary Science Letters* 371–372: 82–91.

Dietze, M., Kreutzer, S., Burow, C., Fuchs, M.C., Fischer, M. & Schmidt, C., 2016. The Abanico plot: visualising chronometric data with individual standard errors. *Quaternary Geochronology* 31: 12–18.

Galbraith, R.F. & Green, P.F., 1990. Estimating the component ages in a finite mixture. *Nuclear Tracks and Radiation Measurements* 17: 197–206.

Galbraith, R.F., Roberts, R.G., Laslett, G.M., Yoshida, H. & Olley, J.M., 1999. Optical dating of single and multiple grains of quartz from Jinmium rock shelter, northern Australia: part 1, experimental design and statistical models. *Archaeometry* 41: 339–364.

Gill, E.D. & Amin, B.S., 1975. Interpretation of 7.5 and 4 metre Last Interglacial shore platforms in southeast Australia. *Search* 6: 394–396.

Gillespie, R., 2002. Dating the first Australians. *Radiocarbon* 44: 455–472.

Goede, A., 1989. Electron spin resonance: a relative dating technique for Quaternary sediments near Warrnambool, Victoria. *Australian Geographical Studies* 27(1): 14–30.

Grün, R., 2009. The 'Age' programme for the calculation of luminescence age estimates. *Ancient TL* 27: 45–46.

Hamm, G., Mitchell, P., Arnold, L.J., Prideaux, G.J., Questiaux, D., Spooner, N.A., Levchenko, V.A., Foley, E.C., Worthy, T.H., Stephenson, B., Coulthard, V., Coulthard, C., Wilton, S. & Johnston, D., 2016. Cultural innovation and megafauna interaction in the early settlement of arid Australia. *Nature*, 539, Issue 7628, 10 November, 280–297.

Haws, J.A., Funk, C.L., Benedetti, M.M., Bicho, N.F., Daniels, J.M., Minckley, T.A., Denniston, R.F., Jeraj, M., Gibaja, J.F., Hockett, B.S. & Forman, S.L., 2011. Paleolithic landscapes and seascapes of the west coast of Portugal. In *Trekking the Shore: Changing Coastlines and the Antiquity of Coastal Settlement*, N.F. Bicho, J.A. Haws, L.G. Davis, eds. Springer Science+Business Media, New York, pp. 203–246.

Hearty, P.J., Hollin, J.T., Neumann, A.C., O'Leary, M.J. & McCulloch, M., 2007. Global sea-level fluctuations during the Last Interglacial (MIS 5e). *Quaternary Science Reviews* 26: 2090–2112.

Hellstrom, J., 2003. Rapid and accurate U-Th dating using parallel ion-counting multi-collector ICP-MS. *Journal of Analytical Atomic Spectrometry* 18: 1346–135.

Hellstrom, J., 2006. U–Th dating of speleothems with high initial ^{230}Th using stratigraphical constraint. *Quaternary Geochronology* 1: 289–295. doi: 10.1016/j.quageo.2007.01.004

Herczeg, A.L. & Chapman, A., 1991. Uranium-series dating of lake and dune deposits in southeastern Australia: a reconnaissance. *Palaeogeography, Palaeoclimatology and Palaeoecology* 84: 285–298.

Hillaire-Marcel, C., Gariépy, C., Ghaleb, B., Goy, J.-L., Zazo, C., Cuerda Barcelo, J., 1996. U-series measurements in Tyrrhenian deposits from Mallorca: further evidence for two last-interglacial high sea levels in the Balearic Islands. *Quaternary Science Reviews* 15: 53–62.

Jacobs, Z., Duller, G.A.T. & Wintle, A.G., 2006. Interpretation of single grain D_e distributions and calculation of D_e. *Radiation Measurements* 41: 264–277.

Kaufman, A., Broecker, W.S., Ku, T.-L. & Thurber, D.L., 1971. The status of U-series methods of mollusk dating. *Geochimica et Cosmochimica Acta* 35: 1155–1183.

Kaufman, D.S. & Manley, W.F., 1998. A new procedure for determining DL amino acid ratios in fossils using reverse phase liquid chromatography. *Quaternary Science Reviews* 17: 987–1000.

Kelly, M., Black, S. & Rowan, J.S., 2000. A calcrete-based U–Th chronology for landform evolution in the Sorbas basin, southeast Spain. *Quaternary Science Reviews* 19: 995–1010.

Lambeck, K. & Chappell, J., 2001. Sea level change through the last glacial cycle. *Science* 292: 679–686.

Lian, O.B. & Roberts, R.G., 2006. Dating the Quaternary: progress in luminescence dating of sediments. *Quaternary Science Reviews* 25: 2449–2468.

Luebbers, R.A., 1978. *Meals and Menus: A Study of Change in Prehistoric Coastal Settlements in South Australia*. PhD Thesis, Australian National University, Canberra, Australia.

Murray, A.S. & Wintle, A.G., 2000. Luminescence dating of quartz using an improved single-aliquot regenerative dose protocol. *Radiation Measurements* 32: 57–73.

Murray-Wallace, C.V., Bourman, R.P., Prescott, J.R., Williams, F., Price, D.M. & Belperio, A.P., 2010. Aminostratigraphy and thermoluminescence dating of coastal aeolianites and the later Quaternary history of a failed delta: the River Murray Mouth region, South Australia. *Quaternary Geochronology* 5: 28–49.

Murray-Wallace, C.V. & Woodroffe, C.D., 2014. *Quaternary Sea-Level* Changes*: A Global Perspective*, Cambridge University Press, Cambridge, 484 pp [Hardback: ISBN: 9780521820837].

Murray-Wallace, C.V., Belperio, A.P., Dosseto, A., Nicholas, A., Mitchell, C., Bourman, R.P., Eggins, S.M. & Grün, R., 2016. Last interglacial (MIS 5e) sea-level determined from a tectonically stable, far-field location, Eyre Peninsula, southern Australia. *Australian Journal of Earth Sciences* 63: 611–630.

Nair, H. & Sherwood, J., 2007. An unusual shell bed at Point Ritchie, Warrnambool, Victoria: predator midden or natural shell bed? *Proceedings of the Royal Society of Victoria* 119(1): 69–86.

Oyston, B., 1996. Thermoluminescence dating of quartz from Quaternary aeolian sediments in southeastern Australia. PhD thesis, La Trobe University, Bundoora, Victoria.

Paton, C., Hellstrom, J., Paul, B., Woodhead, J. & Hergt, J., 2011. Iolite: freeware for the visualisation and processing of mass spectrometer data. *Journal of Analytical Atomic Spectrometry* 26: 2508–2518.

Paton, T.R., Humphreys, G.S. & Mitchell, P.B., 1995. *Soils: A New Global View*. UCL Press Ltd., London. Ch 3: Bioturbation, pp 33–67.

Penkman, K.E.H., Preece, R.C., Bridgland, D.R., Keen, D.H., Meijer, T., Parfitt, S.A., White, T.S. & Collins, M.J., 2013. An aminostratigraphy for the British Quaternary based on *Bithynia* opercula. *Quaternary Science Reviews* 61: 111–134.

Pietsch, T., 2009. Optically stimulated luminescence dating of young (<500 years old) sediments: testing estimates of burial dose. *Quaternary Geochronology* 4: 406–422.

Prescott, J.R. & Sherwood, J.E., 1988. Thermoluminescence ages for an unusual shell deposit at Point Ritchie, Warrnambool, Australia. In *Archaeometry: Australasian Studies 1988,* J.R. Prescott, ed. Department of Physics and Mathematical Physics, The University of Adelaide, Adelaide, 5005, Australia, pp. 61–69.

Prescott, J.R. & Hutton, J.T., 1994. Cosmic ray contribution to dose rates for luminescence and ESR dating: large depths and long-term variations. *Radiation* Measurements 23: 497–500.

Richards, D. & Dorale, J., 2003. Uranium-series chronology and environmental applications of speleothems. *Reviews in Mineralogy and Geochemistry* 52: 407–460.

Schwarz, G.E., 1978. Estimating the dimension of a model. *Annals of Statistics* 6(2): 461–464.

Sherwood, J., Barbetti, M., Ditchburn, R., Kimber, R.W.L., McCabe, W., Murray-Wallace, C.V., Prescott, J.R. & Whitehead, N., 1994. A comparative study of Quaternary dating techniques applied to sedimentary deposits in southwest Victoria, Australia. *Quaternary Geochronology (Quaternary Science Reviews)* 13: 95–110.

Sherwood, J., Oyston, B. & Kershaw, A.P., 2004. The age and contemporary environments of Tower Hill volcano, southwest Victoria, Australia. *Proceedings of the Royal Society of Victoria* 116(1): 69–76.

Spooner N. & Questiaux D. 2015. *Report on optical dating of four samples from Moyjil (formerly Point Ritchie), Warrnambool, Victoria*. Prescott Environmental Luminescence Laboratory, School of Physical Sciences, University of Adelaide, 22 pp.

Valentine, J.W., 1965. Quaternary mollusca from Port Fairy, Victoria, Australia, and their palaeoecologic implications. *Proceedings of the Royal Society of Victoria* 78(1): 15–70.

Woodhead, J., Hergt, J., Shelley, M., Eggins, S. & Kemp, R., 2004. Zircon Hf-isotope analysis with an excimer laser, depth profiling, ablation of complex geometries, and concomitant age estimation. *Chemical Geology* 209: 121–135.

Woodhead, J.D., Hellstrom, J., Hergt, J.M., Greig, A. & Maas, R., 2007. Isotopic and elemental imaging of geological materials by laser ablation inductively coupled plasma-mass spectrometry. *Geostandards Newsletter* 31: 331–343.

Woodhead, J.D., Hellstrom, J., Paton, C., Hergt, J.M., Greig, A. & Maas, R., 2008. A guide to depth profiling and imaging applications of LA–ICP–MS. *Mineralogical Association of Canada Short Course Series* 40: 135–145.

WoRMS Editorial Board 2018. World Register of Marine Species. Available from http://www.marinespecies.org at VLIZ. Accessed 2018-09-20. doi:10.14284/170